





Multiwavelength spectral modelling of the candidate neutrino blazar PKS 0735+178

Athira M. Bharathan ¹★, C. S. Stalin ², S. Sahayanathan,^{3,4} Subir Bhattacharyya ^{3,4} and Blesson Mathew ¹

¹Department of Physics and Electronics, CHRIST (Deemed to be University), Bangalore, India, 560029

²Indian Institute of Astrophysics, Block II, Koramangala, Bangalore 560034, India

³Astrophysical Sciences Division, Bhabha Atomic Research Centre, Mumbai 400085, India

⁴Homi Bhabha National Institute, Mumbai 400094, India

Accepted 2024 January 22. Received 2024 January 19; in original form 2023 September 30

ABSTRACT

The BL Lac object PKS 0735+178 was in its historic γ -ray brightness state during 2021 December. This period also coincides with the detection of a neutrino event IC 211208A, which was localized close to the vicinity of PKS 0735+178. We carried out detailed γ -ray timing and spectral analysis of the source in three epochs: (a) quiescent state (E_1), (b) moderate-activity state (E_2), and (c) high-activity state (E_3) coincident with the epoch of neutrino detection. During the epoch of neutrino detection (E_3), we found the largest variability amplitude of 95 per cent. The γ -ray spectra corresponding to these three epochs are well fit by the power-law model and the source is found to show spectral variations with a softer when brighter trend. In epoch E_3 , we found the shortest flux doubling/halving time of 5.75 h. Even though the spectral energy distribution in the moderate-activity state and in the high-activity state could be modelled by the one-zone leptonic emission model, the spectral energy distribution in the quiescent state required an additional component of radiation over and above the leptonic component. Here, we show that a photomeson process was needed to explain the excess γ -ray emission in the hundreds of GeV that could not be accounted for by the synchrotron self-Compton process.

Key words: galaxies: active – galaxies: BL Lacertae objects: individual: PKS 0735+178 – galaxies: jets.

1 INTRODUCTION

Blazars, among the persistent luminous objects in the Universe with luminosity ranging from 10^{42} to 10^{48} erg s⁻¹, are a class of active galactic nuclei (AGNs). They are believed to be powered by the accretion of matter on to supermassive black hole with masses of the order of 10^6 – 10^{10} M_\odot located at the centre of galaxies (Lynden-Bell 1969; Shakura & Sunyaev 1973). Their radiation is dominated by non-thermal processes from relativistic jets that extend from scales of pc to kpc and are oriented close to the line of sight of the observer. They show rapid and large amplitude flux variations across the electromagnetic spectrum on time-scales ranging from minutes to years (Wagner & Witzel 1995; Ulrich, Maraschi & Urry 1997). In addition to flux variations, the optical emission from blazars is highly polarized (Angel & Stockman 1980) with significant polarization variations (Andruchow, Romero & Cellone 2005; Rakshit et al. 2017; Pandey, Rajput & Stalin 2022). They are also believed to be cosmic accelerators and could be the sources of astrophysical neutrinos (Mannheim 1993a; IceCube Collaboration 2018; Plavin et al. 2020; Giommi & Padovani 2021; Bhatta 2022; Buson et al. 2023).

Blazars are conventionally divided into two subclasses, namely flat spectrum radio quasars (FSRQs) and BL Lacertae-type objects

(BL Lacs) based on the optical spectral properties. FSRQs show broad emission lines in their optical spectra, while BL Lacs have either featureless optical spectra or spectra with weak emission lines with equivalent widths lesser than 5 Å. According to Ghisellini et al. (2011), a more physical distinction between FSRQs and BL Lacs could be based on the luminosity of the broad-line region (BLR) with FSRQs having $L_{\text{BLR}}/L_{\text{Edd}} > 5 \times 10^{-4}$. Here, L_{Edd} is the Eddington luminosity given by $L_{\text{Edd}} = 1.3 \times 10^{38} (M/M_\odot)$ erg s⁻¹. The broad-band spectral energy distribution (SED) of blazars displays two prominent peaks. The low-energy component that peaks between the infrared (IR) and X-ray bands is well understood as the synchrotron emission from a relativistic population of electrons in the blazar jet. The origin of the high-energy component, peaking at the MeV–GeV energy range (Fossati et al. 1998), is highly debated with models that promote a radiation scenario involving either leptons or hadrons or a combination of both (Böttcher et al. 2013; Cerruti 2020). Depending on the location of the low-energy synchrotron peak of the SED, blazars are subdivided into low synchrotron peaked ($\nu_{\text{peak}} < 10^{14}$ Hz), intermediate synchrotron peaked ($10^{14} < \nu_{\text{peak}} < 10^{15}$ Hz), and high synchrotron peaked ($\nu_{\text{peak}} > 10^{15}$ Hz) blazars (Abdo et al. 2010). While FSRQs are predominantly low synchrotron peaked blazars, BL Lacs belong to all three classes with a majority of them belonging to the high synchrotron peak category.

In the leptonic emission model of blazar jets, the high-energy emission component is interpreted as the inverse-Compton scattering

* E-mail: athirabharathan1997@gmail.com

of low-energy photons (Abdo et al. 2010). The target low-energy photons for inverse-Compton emission can be the synchrotron photons, commonly referred to as synchrotron self-Compton or SSC (Konigl 1981), or the photons external to the jet called the external Compton or EC (Begelman & Sikora 1987). Under this emission scenario, one would expect to see a close correlation between optical and GeV flux variations since the same electron population is responsible for the emission at these energies. In the hadronic emission model, the high-energy component is interpreted as a result of hadronic processes. Under this scenario, one need not expect to see a correlation between optical and GeV flux variations since different species are responsible for the emission at these energies. However, systematic investigation of the correlation between optical and GeV flux variations has led to varied results with instances of (a) correlation between optical and GeV variations, (b) optical flare without a GeV counterpart, and (c) GeV flare without the corresponding optical counterpart (Rajput et al. 2019, 2021; Rajput, Stalin & Sahayanathan 2020). Thus, correlated studies of flux variations in the optical and GeV band could not constrain the high-energy emission process unambiguously.

Similarly, the correlation observed between the radio and GeV γ -ray fluxes during various activity states supports the region responsible for these emissions to be cospatial. The radio emission is due to synchrotron radiation by the relativistic electrons in the jet, while the GeV emission is due to the inverse-Compton process. Interestingly, often radio variations are found to lag the GeV variations (Max-Moerbeck et al. 2014; Rani et al. 2014; Esposito et al. 2015; Kramarenko et al. 2022; Yuan et al. 2023). This lag may be associated with the slow cooling of the radio-emitting electrons compared to the γ -ray.

In the hadronic model of the high-energy emission from blazar jets, the plausible emission mechanisms can be proton synchrotron (Aharonian 2000) or hadronic cascades (Mannheim 1993b). Accelerated protons on interaction with cold protons or low-energy photons in the surrounding medium could lead to the production of neutrinos as well as high-energy γ -rays (Prince et al. 2024). Additionally, there are now increased evidence of blazars being extragalactic neutrino sources (Buson et al. 2023; Plavin et al. 2023b). The correlation found between the hard X-ray emission and neutrino emission in blazars (Plavin et al. 2023a) tends to suggest that neutrinos are likely to come from highly beamed blazars strong in X-rays. This led to arguments favouring neutrinos being produced in proton-photon interaction. The association of neutrinos with blazars has also revived the investigation on the hadronic origin of high-energy emissions from blazar jets. Therefore, a comparative analysis of the SED characteristics of candidate neutrino blazars during the epoch of neutrino detection and quiescent/other flaring epochs not coincident with neutrino detection could provide the needed constraints on the high-energy emission process in blazars.

The first blazar found to be associated with the detection of neutrinos by the IceCube Collaboration is TXS 0506+056 observed on 2017 September 22 (IceCube Collaboration 2018). The detection of neutrinos was coincident in direction and time with the γ -ray flare from the source. Since then, few blazars have been found to be spatially coincident with the IceCube neutrino events (Paliya et al. 2020; Boettcher et al. 2022; Sahakyan et al. 2023). Generation of broad-band SED of a large sample of neutrino blazars in a homogeneous manner and their systematic modelling can provide the key to enhancing our understanding of the high-energy component in their broad-band SED. We are carrying out such an investigation and in this work we present our results on the source PKS 0735+178.

The intermediate synchrotron peaked blazar PKS 0735+178 is one of the brightest BL Lacs in the sky. It was identified as a

BL Lac first by Carswell et al. (1974) and is situated at a redshift of $z = 0.45$ (Rector & Stocke 2001). However, recently Falomo, Treves & Paiano (2021) suggest a redshift of $z = 0.65$. It was detected in the γ -rays by the Energetic Gamma Ray Experiment Telescope onboard the *Compton Gamma Ray Observatory* (Hartman et al. 1999) and is also detected by the *Fermi Gamma-ray Space Telescope* (hereafter *Fermi*; Abdollahi et al. 2020). Recently, it was found to be in spatial coincidence with multiple neutrino events by IceCube (IceCube Collaboration 2021), Baikal (Dzhilkibaev, Suvorova & Baikal-GVD Collaboration 2021), Baksan (Petkov et al. 2021), and KM3NeT (Filippini et al. 2022) detectors. This detection of neutrinos by multiple detectors was coincident with the largest flare ever observed in this source in the optical, ultraviolet (UV), soft X-ray, and γ -ray bands. In this work, we carried out a detailed analysis of this source, including the variability, gamma-ray spectral study, and broad-band SED analysis with the help of multiwavelength data. We also modelled the broad-band SEDs using a simple one-zone leptonic model, and the discrepancy of this model in explaining the γ -ray spectrum is inferred with the hadronic photomeson process. This paper is organized as follows: multiwavelength data and reduction are described in Section 2; the analysis, results, and the broad-band spectral fitting are discussed in Section 3; and the results of this work are summarized in Section 4. Throughout this paper, we used the cosmological constants $\Omega_M = 0.3$, $\Omega_\Lambda = 0.7$, and $H_0 = 71 \text{ km s}^{-1} \text{ Mpc}^{-1}$.

2 MULTIWAVELENGTH DATA AND REDUCTION

The observational data used in this work were from the Large Area Telescope (LAT; Atwood et al. 2009) onboard the *Fermi* over the period of about 14 yr from 2008 August to 2022 February. In addition to the γ -ray data, we also used UV, optical, and X-ray data covering the same period from the *Swift* telescope.

2.1 γ -ray

We used all data for PKS 0735+178 collected for the period 2008 August to 2022 February (MJD 54749–59611) from the *Fermi* archives. We utilized the FERMIPY package (Wood et al. 2017),¹ a PYTHON package that facilitates analysis of data from the LAT with the *Fermi* Science Tools for the generation of spectral points. We extracted photon-like events categorized as ‘evclass=128, evttype=3’ with energies $0.1 \leq E \leq 300 \text{ GeV}$ γ -rays within a circular region of interest of 15° centred on the source. We applied the recent isotropic emission model ‘iso_P8R2_SOURCE_V6.v06’ and the Galactic diffuse emission model ‘gll_iem.v06’. For generation of the γ -ray light curves, we considered the source to be detected if the test statistics (TS) > 9 , which corresponds to a 3σ detection (Mattox et al. 1996). For bins with $TS < 9$, we considered the source as undetected.

2.2 X-ray

We used data from the *Swift*/X-Ray Telescope (XRT) collected from the HEASARC² archives for X-rays with energies between 0.3 and 10 keV from 2008 August to 2022 February. We reduced the data using the default parameter values in accordance with the instructions provided by the instrument team. The source spectra

¹<https://fermipy.readthedocs.io/en/latest/>

²<https://heasarc.gsfc.nasa.gov/docs/archive.html>

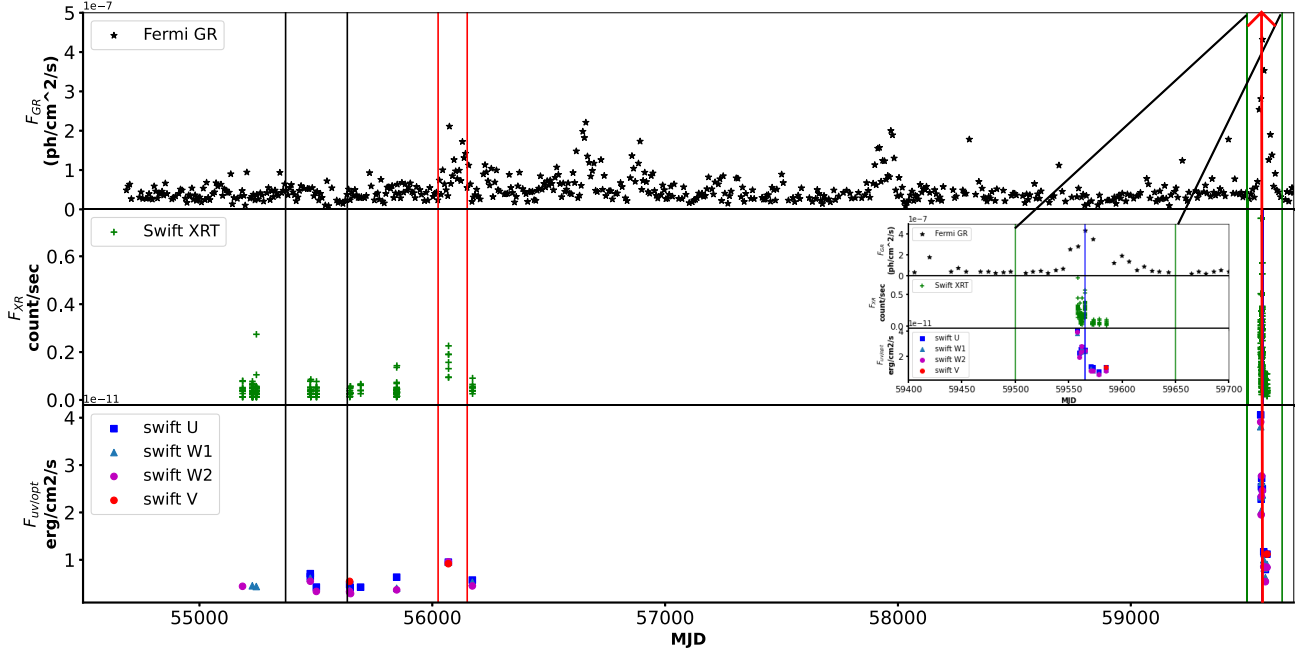


Figure 1. Multiwavelength light curves of the source PKS 0735+178. From the top, the first panel shows the weekly binned γ -ray light curve for the time range MJD 54749–59611; the second panel shows the *Swift*-XRT light curve in photon counting mode; and the third panel shows the *Swift*-UVOT light curves in W1, W2, U, and V bands. The arrowed vertical line is the epoch of neutrino detection. The regions encompassed by the first two vertical lines, next two vertical lines, and the last two vertical lines refer to epochs E_1 , E_2 , and E_3 , respectively. The inset is the zoomed region around the flaring epoch E_3 .

Table 1. The γ -ray fractional variability amplitude (F_{var}) in different epochs in the 100 MeV to 300 GeV band. Here, E_1 corresponds to the quiescent state, E_2 corresponds to the active state, and E_3 corresponds to the high state of the source that coincides with the neutrino detection.

Epoch	F_{var} (per cent)
E_1	–
E_2	41.3 ± 7.9
E_3	95.2 ± 6.5
Total LC	61.9 ± 4.3

were chosen from a region of radii 60 arcsec, whereas the background spectra were taken from a region of radii 120 arcsec. We combined the exposure map using the tool XIMAGE and created the ancillary response files with XRTMKARF. We used an absorbed simple power-law model with the Galactic neutral hydrogen column density of $3.74 \times 10^{20} \text{ cm}^{-2}$ to perform the fitting within XSPEC (Arnaud 1996).

2.3 UV and optical

For the analysis of UV and optical data from 2008 August to 2022 February, we utilized the data obtained from the *Swift*-Ultraviolet and Optical Telescope (UVOT), an instrument onboard the *Swift* spacecraft. We used the data from the filters V, U, W1, and W2. The central wavelength (full width at half-maximum) of these filters is 5468 Å (796 Å), 3465 Å (785 Å), 2600 Å (693 Å), and 1928 Å (657 Å) (Poole et al. 2008). We processed the data from *Swift*-UVOT using the online tool provided by the telescope’s data archive. In order to account for the effects of galactic absorption, we applied corrections to the UV and optical data points during SED analysis.

3 ANALYSIS AND RESULTS

3.1 Multiwavelength light curve

We utilized the 1-week binned γ -ray light curve in the 100 MeV to 300 GeV band generated using the procedure outlined in Section 2.1. The multiwavelength light curves spanning about 14 yr that include γ -ray, X-ray, UV, and optical from 2008 August to 2022 February (MJD 54749–59611) are shown in Fig. 1. From Fig. 1, it is evident that PKS 0735+178 has gone through both quiescent and active phases. During this period, we identified three time intervals. They are denoted as epochs E_1 , E_2 , and E_3 . E_1 covers the period MJD 55370–55635 (265 d), when the source was in a quiescent state; E_2 covers the period MJD 56025–56150 (125 d), when the source was in an active state; and E_3 covers the period MJD 59500–59650 (150 d), when the source was in a historically high state coincident with the epoch of neutrino detection. The neutrino event detected on 2021 December 8 (MJD 59556) is marked as a blue vertical line in Fig. 1 in E_3 . During this epoch, the source showed the largest flare ever observed in the optical, UV, X-rays, and γ -rays.

3.2 Variability analysis

3.2.1 Long-term variability

To quantify the variability of the source on time-scales of weeks, we calculated the fractional variability amplitude (F_{var}) in different energy bands following Vaughan et al. (2003). We define

$$F_{\text{var}} = \sqrt{\frac{S^2 - \sigma_{\text{err}}^2}{\bar{x}^2}}, \quad (1)$$

where S^2 is the variance, \bar{x} is the mean, and σ_{err}^2 is the mean square of the measurement error on the flux points. The uncertainty on F_{var}

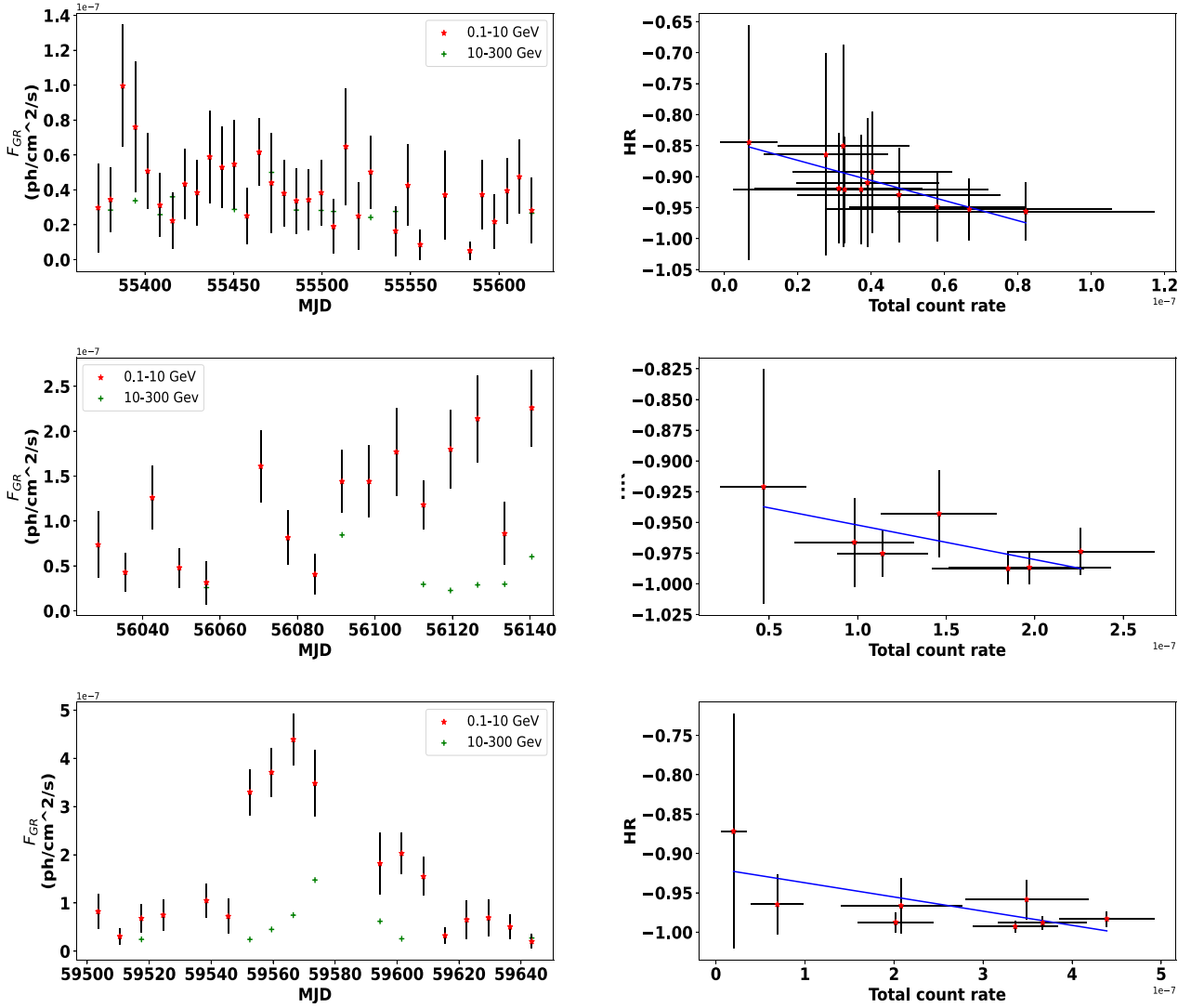


Figure 2. Left panels: 1-week binned γ -ray light curves for epochs E_1 (top-left), E_2 (middle-left), and E_3 (bottom-left) in the 0.1–10 GeV (red) and 10–300 GeV multiplied by a factor of 20 (green). Right panels: HR versus total intensity in the 0.1–300 GeV band for epochs E_1 (top-right), E_2 (middle-right), and E_3 (bottom-right). Here the solid lines are the weighted linear least-squares fit to the data.

Table 2. Results of the weighted linear least-squares fit to the HR versus total intensity diagram. Here, epochs E_1 , E_2 , and E_3 correspond to the quiescent, active, and high state of the source, R is the linear correlation coefficient, and p is the probability for no correlation.

Epochs	Slope ($\times 10^7$)	Intercept	R	p
E_1	-0.16 ± 0.01	-0.84 ± 0.02	-0.83	0.001
E_2	-0.03 ± 0.01	-0.92 ± 0.02	-0.72	0.066
E_3	-0.02 ± 0.00	-0.92 ± 0.02	-0.69	0.061

is given by (Vaughan et al. 2003)

$$F_{\text{var, err}} = \sqrt{\frac{1}{2N} \left(\frac{\sigma_{\text{err}}^2}{F_{\text{var}} \bar{x}^2} \right)^2 + \frac{1}{N} \frac{\sigma_{\text{err}}^2}{\bar{x}^2}}. \quad (2)$$

Here, N represents the number of flux points in the light curve. We calculated the γ -ray variability for E_1 , E_2 , and E_3 and for the total light curve. The results of the variability analysis are given in Table 1.

3.2.2 Short-term variability

Blazars are known to show γ -ray flux variations on time-scales lesser than an hour (Foschini et al. 2011; Saito et al. 2013; Pandey & Stalin 2022). Detection of such short time-scale variation could enable one to constrain the size and the location of the γ -ray-emission region. We, therefore, searched for the presence of flux variations on very short time-scales (of the order of hours) in the γ -ray light curve of PKS 0735+178. For this, we identified the epoch of very high γ -ray activity, namely, E_3 and generated 1 d binned light curves. We then calculated the flux doubling/halving time-scale using the relation

$$F(t) = F(t_0) \times 2^{-(t-t_0)/\tau}. \quad (3)$$

Here, $F(t)$ and $F(t_0)$ are the fluxes at time t and t_0 , respectively, and τ is the flux doubling/halving time-scale. This calculation was done with the condition that the flux difference between epochs t and t_0 is greater than 3σ (Foschini et al. 2011). Using the flux doubling time-scale, we constrained the size of the γ -ray-emitting region as

$$R \leq \frac{c\tau\delta}{1+z}, \quad (4)$$

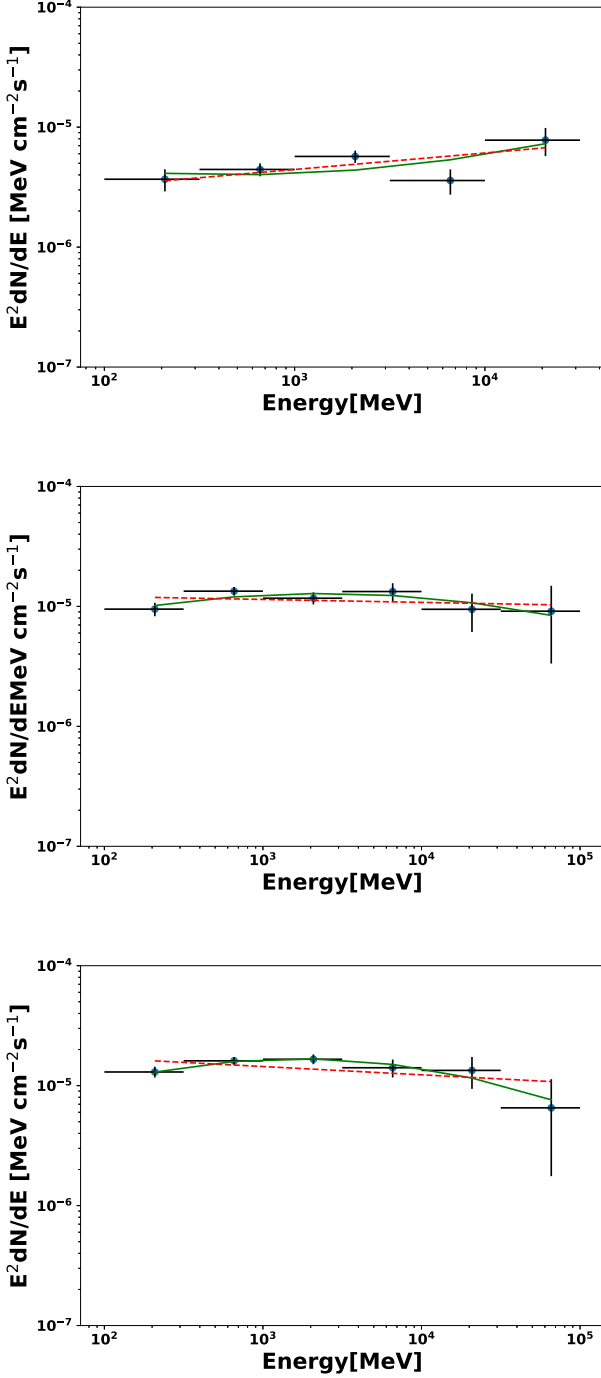


Figure 3. Simple power law (dotted line) and log parabola (solid line) fits to the γ -ray spectra of PKS 0735+178 during epochs E_1 (top panel), E_2 (middle panel), and E_3 (bottom panel).

where δ is the Doppler Factor, τ is the flux doubling/having time-scale, and c is the speed of light.

3.2.3 Spectral variability

To investigate spectral variations in the source, during the epochs analysed in this work, we followed a model-independent approach of estimating the hardness ratio (HR) and then investigated the dependence of HR on the total flux of the source. For this, we

generated 1 d binned γ -ray light curves in two energy ranges, namely, 0.1–10 GeV and 10–300 GeV. We define HR and the associated errors in HR as

$$\text{HR} = \left(\frac{H - S}{H + S} \right), \quad (5)$$

$$\sigma_{\text{HR}} = \frac{2}{(H + S)^2} \sqrt{H^2 \sigma_S^2 + S^2 \sigma_H^2}. \quad (6)$$

The generated light curves in the two energy ranges and the corresponding HR for the three epochs are shown in Fig. 2. From the light curves, it is evident that the hard flux counts are lower compared to the soft flux counts. We carried out a weighted linear least-square fit to the HR versus intensity diagram in Fig. 2. The results of the fit are given in Table 2. We found significant evidence of spectral variation in only one epoch, namely, E_1 , wherein we found a softer when brighter trend. This is at odds with the recent finding of a harder when brighter trend seen in the γ -ray band (Fang et al. 2022). Close to the period of neutrino detection, in the X-ray band the source was found to show a softer when brighter trend, generally seen in the FSRQ category of blazars (Prince et al. 2024).

3.3 γ -ray spectra

The slope of the γ -ray spectrum can provide hints on the intrinsic accelerated electron distribution responsible for this emission process. We carried out the analysis of the γ -ray spectra of the three epochs using two spectral models namely the power law (PL) and log parabola (LP) models. The PL model has the functional form as

$$\frac{dN(E)}{dE} = N_0 E^{-\Gamma}. \quad (7)$$

Here, $dN(E)/dE$ is the differential photon number ($\text{cm}^{-2} \text{s}^{-1} \text{MeV}^{-1}$), N_0 is the normalization, and Γ is the photon index. The LP model is defined as (Nolan et al. 2012)

$$dN(E)/dE = N_0 (E/E_0)^{-\alpha - \beta \ln(E/E_0)}, \quad (8)$$

where α is photon spectral slope at energy E_0 , and β defines the peak spectral curvature of the SED. We used the maximum likelihood estimator *glike* and the likelihood ratio test (Mattox et al. 1996) to check the PL model (null hypothesis) against the LP model (alternative hypothesis). We calculated the curvature of test statistics $\text{TS}_{\text{curve}} = 2(\log L_{\text{LP}} - \log L_{\text{PL}})$ following Nolan et al. (2012). We tested the presence of a significant curvature by setting the condition $\text{TS}_{\text{curve}} > 16$. The γ -ray spectra along with the model fits for epochs E_1 , E_2 , and E_3 are shown in Fig. 3. The parameters of the fit are given in Table 3. Significant curvature in the γ -ray spectrum is not found in the three epochs.

3.4 Broad-band SED analysis

We modelled the generated SEDs of the three epochs using the one-zone leptonic model (Sahayanathan, Sinha & Misra 2018). In this model, the emission region was assumed to be a spherical blob of size R filled with non-thermal electrons following a broken power-law distribution:

$$N(\gamma) d\gamma = \begin{cases} K \gamma^{-p} d\gamma & \text{for } \gamma_{\min} < \gamma < \gamma_b, \\ K \gamma_b^{q-p} \gamma^{-q} d\gamma & \text{for } \gamma_b < \gamma < \gamma_{\max}, \end{cases} \quad (9)$$

where γ is the electron Lorentz factor, and p and q are the low- and high-energy power-law indices with γ_b the Lorentz factor corresponding to the break energy. The emission region is permeated with a tangled magnetic field B and moves down the jet with a

Table 3. Results of the power law (PL) and log parabola (LP) model fits to the three epochs E_1 , E_2 , and E_3 . Here, E_1 , E_2 , and E_3 represent the quiescent, active, and high state of the source. Here, Γ is the photon index, flux is the γ -ray flux value in units of 10^{-12} photons $\text{cm}^{-2} \text{s}^{-1}$, TS is the test statistics, α is the spectral index, β is the curvature in the spectra, and TS_{curve} signifies the presence of curvature in the spectra.

Epochs	PL					LP				
	Γ	Flux	TS	L_{PL}	α	β	Flux	TS	L_{LP}	TS_{curve}
E_1	-1.99	2.006	637.221	-44224.847	1.94 ± 0.07	0.07 ± 0.04	2.162	634.591	-44225.597	-1.5
E_2	-2.01	5.234	1050.448	-26527.641	1.99 ± 0.05	0.07 ± 0.03	5.887	958.9225	-26524.141	7.00
E_3	-2.01	6.453	1381.112	-25249.253	2.01 ± 0.05	0.07 ± 0.03	7.319	1359.155	-25246.537	5.43

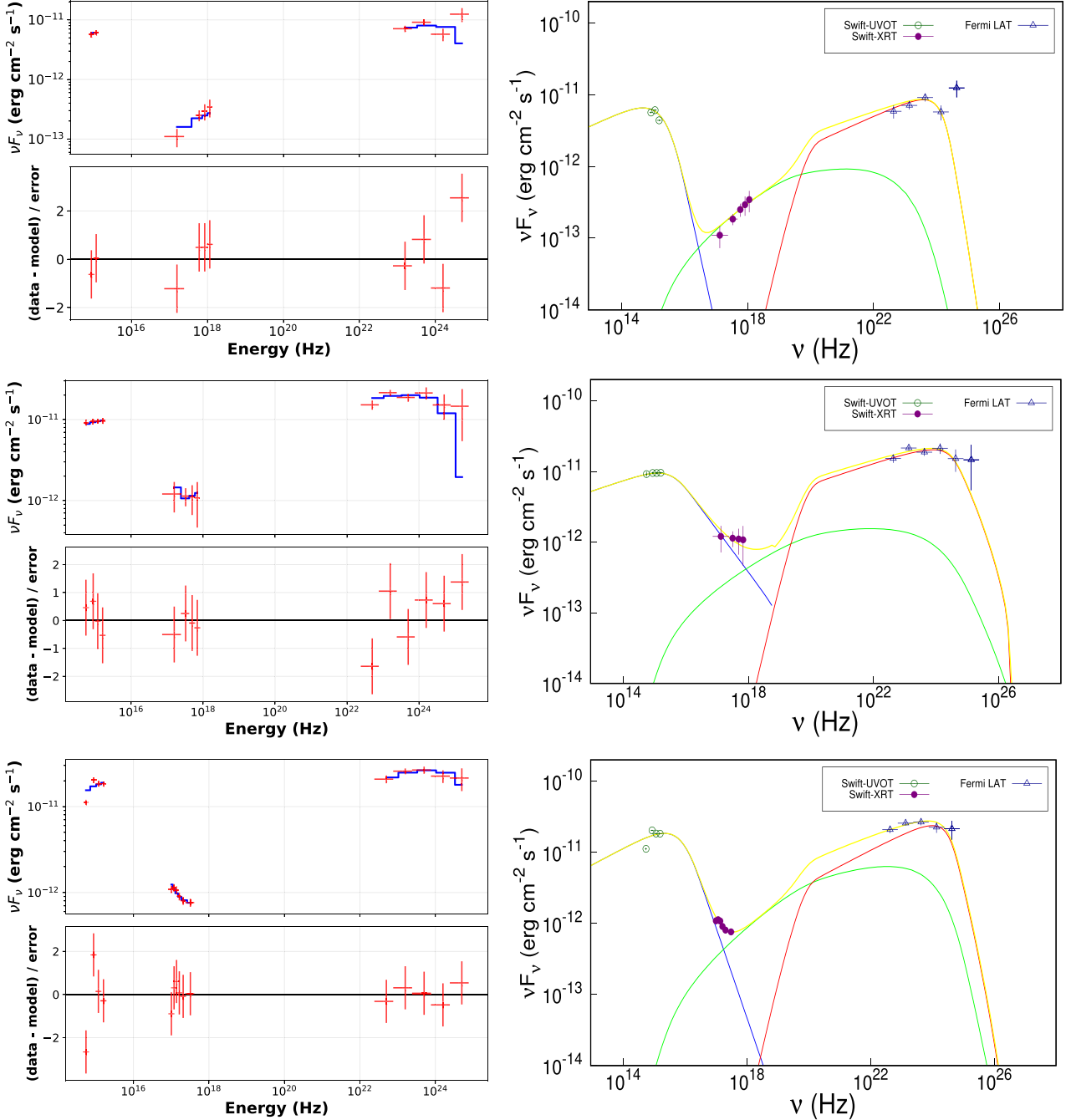


Figure 4. Broad-band SED along with the one-zone leptonic emission model fits for E_1 (top panel), E_2 (middle panel), and E_3 (bottom panel). In the right panels, the synchrotron model, the SSC process, and the EC process are shown. The line which passes through all the points refers to the sum of all the components. In the left panels for each epoch, the first panel shows the fitting of the model to the data and the second panel shows the residuals carried out in XSPEC.

Table 4. Results of the broad-band SED analysis carried out for epochs E_1 , E_2 , and E_3 . Here, E_1 represents the quiescent state, E_2 represents the active state, and E_3 represents the high state of the source. The parameters p and q are the low- and high-energy power-law indices of the electron distribution, γ_b is the break energy, R is the size of the emission blob in cm, Γ is the bulk Lorentz factor, and B is the magnetic field in G.

Parameter	E_1	E_2	E_3
p	2.60	2.70	2.58
q	7.0	4.40	5.57
γ_b	7063	8067	12339
$\log(R)$ (cm)	16.4	16.2	16.4
Γ	11.3	23.1	11.2
B (G)	0.65	0.68	0.74

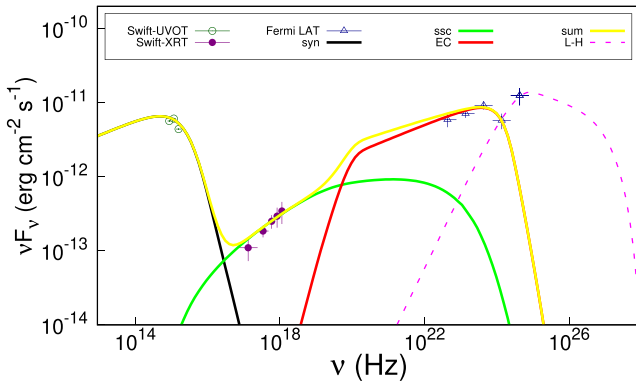


Figure 5. Broad-band SED along with the one-zone leptonic emission model fits for E_1 with the inclusion of the photomeson process. The synchrotron emission line, the EC emission line, the SSC emission line, and the sum of all these are represented. The photomeson process is shown by the dotted line.

bulk Lorentz factor Γ . The broad-band SEDs were modelled using synchrotron, SSC, and EC emission mechanisms. XSPEC modelled SEDs of the source PKS 0735+178 for the selected epochs E_1 , E_2 , and E_3 are shown in Fig. 4. The numerical model is coupled with a local model in X-ray spectral fitting package XSPEC (Arnaud 1996) and the fitting was performed. We found from the fitting that the γ -ray emission is better explained by the EC process with the target photons from the IR dusty torus at a temperature of 1000 K. The best-fitting parameters obtained are listed in Table 4. The best-fitting model along with the observed data is shown in Fig. 4. Though classified as a BL Lac object, the broad-band SED of PKS 0735+178 resembles that of a FSRQ with the requirement of EC process to explain the observed high-energy emission. This is also similar to the case of the first high-energy neutrino blazar TXS 0506+056, which was found not a BL Lac but a FSRQ (Padovani et al. 2019). The requirement of the external target photon field to explain the observed SED in PKS 0735+178 as found here has also been hinted recently (Acharyya et al. 2023; Sahakyan et al. 2023).

For all the epochs except E_1 , the spectral fit satisfies all the γ -ray flux points. The highest γ -ray flux point of E_1 corresponding to energy 21 GeV cannot be explained under the leptonic model, and we investigated this by considering the additional emission from the photomeson process. In this lepto-hadronic model, we considered the interaction of relativistic protons with the synchrotron photons.

We considered a particle distribution involving a combination of leptons and hadrons to model the excess high-energy emission in E_1 . The contribution of these protons is subdominant in the

lower energy region. We considered a photomeson process in which relativistic protons interact with the synchrotron photons. In this model, we only considered the production of π^0 meson and its decay into two γ photons. We used the model developed by Kelner & Aharonian (2008) to incorporate the photomeson emission process in the modelling of the SED of E_1 . The energy distribution of γ -rays produced by the decay of π^0 meson is given by

$$\frac{dN_\gamma}{dE_\gamma} = \int f_p(E_p) f_{ph}(\epsilon) \phi_\gamma(\eta, x) \frac{dE_p}{dE_p} d\epsilon, \quad (10)$$

where

$$f_p(E_p) dE_p$$

and

$$n_{ph}(\epsilon) d\epsilon$$

are the proton and photon number densities in the energy ranges dE_p and $d\epsilon$, respectively.

Epoch E_1 is remodelled by including a photomeson process and shown in Fig. 5.

4 SUMMARY

In this work, we carried out γ -ray spectral, timing, and multiband SED analysis of the neutrino blazar PKS 0735+178 based on γ -ray data collected over a period of 14 yr. The main motivation is to see how the broad-band SED of the blazar during the neutrino detection epoch compares with the SED of the same source generated at other epochs. The results are summarized below.

(i) The source was in its historic brightness state in the γ -ray band during E_3 . During this period, a neutrino event was localized close to the vicinity of PKS 0735+178. During this period, in addition to its brightness state in the γ -ray band, it also flared in the UV, optical, and X-ray bands.

(ii) From variability analysis of the three epochs, we found a maximum F_{var} of 95 per cent during epoch E_3 .

(iii) On shorter time-scales, we found a flux doubling/halving time-scale of 5.75 h, and the size of the γ -ray-emission region is estimated to be 8.22×10^{15} cm.

(iv) The γ -ray spectra during all three epochs are well fit with the PL model. The photon indices obtained by the PL model fit to all three epochs range between 1.9 and 2. This is similar to that known for BL Lacs (Singal 2015), however, it is harder when compared to FSRQs.

(v) We found the source to show spectral variations. A moderately softer when brighter trend was noticed in all three epochs.

(vi) The SED modelling of epochs E_2 and E_3 leads to the conclusion that the observed γ -ray emission is due to inverse-Compton scattering of thermal IR photons by relativistic jet electrons. Even during the epoch of neutrino detection, the SED of PKS 0735+178 can be well modelled under the pure leptonic emission scenario. Probably during this epoch, the hadronic emission contribution is subdominant to the leptonic process. This is consistent with Sahakyan et al. (2023), where the authors showed that the SED of PKS 0735+178 during the neutrino detection epoch was lepton dominated.

(vii) The leptonic model alone was unable to reproduce the quiescent state γ -ray spectrum; however, a combination with the photomeson process suggests significant improvement in the spectral fit. This suggests that the source PKS 0735+178 has a non-negligible hadronic emission contribution during its quiescent state, but during

the flaring periods E_2 and E_3 leptonic process dominates over the hadronic process.

With the identification of the association of neutrinos with more blazars, followed by multiband data accumulation and SED modelling, it would be possible to constrain the leptonic and/or hadronic origin of the high-energy γ -ray emission in blazars.

ACKNOWLEDGEMENTS

AMB acknowledges the Department of Science and Technology (DST) for the INSPIRE Fellowship (IF200255) and thanks the Centre for Research, CHRIST (Deemed to be University) for all their support during the course of this work. Special appreciation is extended to Bhoomika Rajput for her dedicated assistance. In this work, we have used the archival γ -ray data from *Fermi* Science Support Center (FSSC). We have also used the *Swift*-XRT/UVOT data from the High Energy Astrophysics Science Archive Research Center (HEASARC).

DATA AVAILABILITY

All the data used here for analysis are publicly available and the results are incorporated in the paper.

REFERENCES

- Abdo A. et al., 2010, *ApJ*, 716, 30
 Abdollahi S. et al., 2020, *ApJS*, 247, 33
 Acharyya A. et al., 2023, *ApJ*, 954, 70
 Aharonian F. A., 2000, *New Astron.*, 5, 377
 Andruchow I., Romero G. E., Cellone S. A., 2005, *A&A*, 442, 97
 Angel J. R. P., Stockman H. S., 1980, *ARA&A*, 18, 321
 Arnaud K. A., 1996, in Jacoby G. H., Barnes J., eds, ASP Conf. Ser. Vol. 101, Astronomical Data Analysis Software and Systems V. Astron. Soc. Pac., San Francisco, p. 17
 Atwood W. B. et al., 2009, *ApJ*, 697, 1071
 Begelman M. C., Sikora M., 1987, *ApJ*, 322, 650
 Bhatta G., 2022, *Universe*, 8, 513
 Boettcher M., Fu M., Govenor T., King Q., Roustazadeh P., 2022, preprint (arXiv:2204.12242)
 Böttcher M., Reimer A., Sweeney K., Prakash A., 2013, *ApJ*, 768, 54
 Buson S. et al., 2023, preprint (arXiv:2305.11263)
 Carswell R. F., Strittmatter P. A., Williams R. E., Kinman T. D., Serkowski K., 1974, *ApJ*, 190, L101
 Cerruti M., 2020, *Galaxies*, 8, 72
 Dzhilkibaev Z. A., Suvorova O., Baikal-GVD Collaboration, 2021, Astron. Telegram, 15112, 1
 Esposito V., Walter R., Jean P., Tramacere A., Türler M., Lähtenmäki A., Tornikoski M., 2015, *A&A*, 576, A122
 Falomo R., Treves A., Paiano S., 2021, Astron. Telegram, 15132, 1
 Fang Y., Chen Q., Zhang Y., Wu J., 2022, *ApJ*, 933, 224
 Filippini F. et al., 2022, Astron. Telegram, 15290, 1
 Foschini L., Ghisellini G., Tavecchio F., Bonnoli G., Stamerra A., 2011, *A&A*, 530, A77
 Fossati G., Maraschi L., Celotti A., Comastri A., Ghisellini G., 1998, *MNRAS*, 299, 433

- Ghisellini G., Tavecchio F., Foschini L., Ghirlanda G., 2011, *MNRAS*, 414, 2674
 Giommi P., Padovani P., 2021, *Universe*, 7, 492
 Hartman R. C. et al., 1999, *ApJS*, 123, 79
 IceCube Collaboration, 2018, *Science*, 361, eaat1378
 IceCube Collaboration, 2021, GCN Circ., 31191, 1
 Kelner S. R., Aharonian F. A., 2008, *Phys. Rev. D*, 78, 034013
 Konigl A., 1981, *ApJ*, 243, 700
 Kramarenko I. G., Pushkarev A. B., Kovalev Y. Y., Lister M. L., Hovatta T., Savolainen T., 2022, *MNRAS*, 510, 469
 Lynden-Bell D., 1969, *Nature*, 223, 690
 Mannheim K., 1993a, *Phys. Rev. D*, 48, 2408
 Mannheim K., 1993b, *A&A*, 269, 67
 Mattox J. R. et al., 1996, *ApJ*, 461, 396
 Max-Moerbeck W. et al., 2014, *MNRAS*, 445, 428
 Nolan P. L. et al., 2012, *ApJS*, 199, 31
 Padovani P., Oikonomou F., Petropoulou M., Giommi P., Resconi E., 2019, *MNRAS*, 484, L104
 Paliya V. S., Böttcher M., Olmo-García A., Domínguez A., Gil de Paz A., Franckowiak A., Garrappa S., Stein R., 2020, *ApJ*, 902, 29
 Pandey A., Rajput B., Stalin C. S., 2022, *MNRAS*, 510, 1809
 Pandey A., Stalin C. S., 2022, *A&A*, 668, A152
 Petkov V. B., Novoseltsev Y. F., Novoseltseva R. V., Baksan Underground Scintillation Telescope Group, 2021, Astron. Telegram, 15143, 1
 Plavin A. V., Burenin R. A., Kovalev Y. Y., Lutovinov A. A., Starobinsky A. A., Troitsky S. V., Zakharov E. I., 2023a, preprint (arXiv:2306.00960)
 Plavin A. V., Kovalev Y. Y., Kovalev Y. A., Troitsky S. V., 2020, Astron. Telegram, 14238, 1
 Plavin A. V., Kovalev Y. Y., Kovalev Y. A., Troitsky S. V., 2023b, *MNRAS*, 523, 1799
 Poole T. S. et al., 2008, *MNRAS*, 383, 627
 Prince R., Das S., Gupta N., Majumdar P., Czerny B., 2024, *MNRAS*, 527, 8746
 Rajput B., Shah Z., Stalin C. S., Sahayanathan S., Rakshit S., 2021, *MNRAS*, 504, 1772
 Rajput B., Stalin C. S., Sahayanathan S., 2020, *MNRAS*, 498, 5128
 Rajput B., Stalin C. S., Sahayanathan S., Rakshit S., Mandal A. K., 2019, *MNRAS*, 486, 1781
 Rakshit S., Stalin C. S., Muneer S., Neha S., Paliya V. S., 2017, *ApJ*, 835, 275
 Rani B., Krichbaum T. P., Marscher A. P., Jorstad S. G., Hodgson J. A., Fuhrmann L., Zensus J. A., 2014, *A&A*, 571, L2
 Rector T. A., Stocke J. T., 2001, *AJ*, 122, 565
 Sahakyan N., Giommi P., Padovani P., Petropoulou M., Bégué D., Boccardi B., Gasparian S., 2023, *MNRAS*, 519, 1396
 Sahayanathan S., Sinha A., Misra R., 2018, *Res. Astron. Astrophys.*, 18, 035
 Saito S., Stawarz Ł., Tanaka Y. T., Takahashi T., Madejski G., D'Ammando F., 2013, *ApJ*, 766, L11
 Shakura N. I., Sunyaev R. A., 1973, *A&A*, 24, 337
 Singal J., 2015, *MNRAS*, 454, 115
 Ulrich M.-H., Maraschi L., Urry C. M., 1997, *ARA&A*, 35, 445
 Vaughan S., Edelson R., Warwick R. S., Uttley P., 2003, *MNRAS*, 345, 1271
 Wagner S. J., Witzel A., 1995, *ARA&A*, 33, 163
 Wood M. et al., 2017, in *35th International Cosmic Ray Conference (ICRC2017)*. International Cosmic Ray Conference, 301, p. 824
 Yuan Q. et al., 2023, *ApJ*, 953, 47

This paper has been typeset from a $\text{\TeX}/\text{\LaTeX}$ file prepared by the author.